SPECTROSCOPY AND DIRECT IMAGING OF THE PLANETARY NEBULA IC 4593[1]

J. Bohigas and L. Olguín

Instituto de Astronomía
Universidad Nacional Autónoma de México

RESUMEN

Espectroscopía de la nebulosa planetaria IC 4593 muestra que las abundancias de helio, oxígeno, carbono, azufre y argón, son típicas de planetarias de tipo distinto al I. La abundancia de nitrógeno es normal si se incluyen datos del UV. El neón es subabundante por un factor de 2. Imágenes en varias líneas de emisión muestran que el objeto está integrado por dos estructuras internas cuya morfología está dominada por efectos hidrodinámicos, rodeadas por un halo grumoso, practicamente esférico, y de alta excitación. Hay muchas condensaciones, la mayor parte mas allá del halo, predominantemente situadas al suroeste de la estrella central y agrupadas en hileras que llegan al cuerpo principal de la planetaria. El flujo en Hβ es 3.1×10^{-11} erg cm^{-2} s^{-1} para toda la nebulosa. El 97% se concentra en la estructura más interna, donde la masa de gas ionizado es $\simeq 0.72(D_{kpc}/4.3)^2$ $M_\odot$ (D_{kpc}, distancia en kpc). El flujo en Hβ en las estructuras centrales es mayor hacia el noroeste. La densidad, temperatura y grado de excitación en la región más interna, cambian con el ángulo acimutal. Presentamos algunas objeciones a la hipótesis que propone que la estructura de las regiones externas de IC 4593 situadas al noroeste, es ocasionada por el movimiento supersónico del objeto. Sugerimos que su morfología puede deberse principalmente a procesos de pérdida de masa de la estrella central.

ABSTRACT

Spectroscopy of the planetary nebula IC 4593 leads to helium, oxygen, carbon, sulfur and argon abundances which are typical of non-type I planetaries. Nitrogen abundance is normal when UV data is used. Neon might be underabundant by a factor of 2. Images in various emission lines show that the nebula is composed of two internal structures dominated by gas dynamical effects, surrounded by a nearly spherical, clumpy and highly excited halo. There are many condensations, mostly beyond the halo, predominantly located to the southwest of the central star, forming sets of strings connected to the object's main body. The Hβ flux for the entire nebula is 3.1×10^{-11} erg cm^{-2} s^{-1}, 97% from the innermost structure, where the mass of ionized gas is $\simeq 0.72(D_{kpc}/4.3)^2$ $M_\odot$ (D_{kpc}, distance in kpc). The Hβ flux in the internal structures is larger to the northwest. The density, temperature and degree of excitation in the innermost region change with the azimuthal angle. We present some objections to the hypothesis that the structure of the outer northwestern region of IC 4593 is caused by supersonic motion into the ISM. We suggest that the morphology of the planetary may be mainly due to different forms of mass loss from the central star.

Key words: **PLANETARY NEBULAE – INDIVIDUAL (IC 4593)**

1. INTRODUCTION

IC 4593 (G025.3+40.8) is an elliptical planetary nebula with clearly defined ansae, an outer faint halo, and a number of condensations extending well beyond its main body (Balick et al. 1992). As discussed by Zucker & Socker (1993), a variety of different type of structures are present in IC 4593, suggesting the concurrence of several distinct physical processess. In particular, they suggest that the NW boundary of the nebula is shaped by its supersonic motion with respect to the ambient medium. The central star had been suspected to be variable for many years (Kazarian 1968). This was confirmed when spectral changes in several emission lines —He II 4686 and the N III, C III and C IV line complex around 4640 Å— were observed on a timescale of a day (Méndez, Herrero, & Manchado 1990). Furthermore, these authors also find significant radial velocity variations of the He II 4541 absorption line in the spectrum of the central star. These changes are thought to be connected to fluctuations in the mass loss rate, a property that is believed to be common in planetaries with comparatively strong winds. The mass loss rate and wind velocity of the central star of IC 4593 are about $4 \times 10^{-8} M_\odot$ yr^{-1} and 1400 km s^{-1} (Hutsemekers & Surdej 1989; Cerruti-Sola & Perinotto 1989). According to Méndez et al. (1990), the spectral type of the central star is O5f, has an effective temperature of 40 000 K and is 3.5 kpc distant. Cudworth (1974) finds a distance of 4.3 kpc, which would imply that it is very far from the plane, $z \simeq 2.8$ kpc. He also derives a relatively large proper motion for the object ($\mu_\alpha = -35 \pm 17$, $\mu_\delta = 76 \pm 24 \times 10^{-4}$ arcsec yr^{-1}). There are many other distance estimates (see Acker et al. 1992) the smallest one being 1.5 kpc (Amnuel et al. 1984). Thus, the object is at least 1 kpc distant from the galactic plane. Spectroscopic observations of the nebula have been carried out in the optical and IR domains (Peimbert & Torres-Peimbert 1971; Perinotto 1974; Lutz 1977; Czyzak, Buerger, & Aller 1975; Barker 1978; Dinerstein 1980; Freitas-Pacheco et al. 1989). These works lead to very low oxygen, neon and argon abundances, but there are conflicting reports regarding the abundance of nitrogen and sulfur. On the other hand, French (1983) derives a normal carbon abundance.

Since most previous spectroscopic observations conveyed information on a limited number of lines (Peimbert & Torres-Peimbert 1971; Perinotto 1974; Lutz 1977; Dinerstein 1980), and others lead to conflicting results in a number of them (Czyzak et al. 1975; Barker 1978), we decided to carry out spectroscopic observations from 3450 to 9200 Å. These observations were combined with existing UV and IR data hoping to produce more reliable information on nebular abundances. On the other hand, the analysis of the nebula carried out by Zucker &

Socker (1993) is based on images taken in the light of Hα+[N II] 6584, [O III] 5007 and [S II] 6717, 6731, and most of their attention was diverted to the NW region. In this paper we produce images in several more emission lines, take account of continuum emission (which is very important in faint lines), and calibrate them using our spectral results. Thus, we are able to produce density and temperature maps, and evaluate the importance of different ions throughout the nebula, so as to assess the physical conditions of all structures.

2. OBSERVATIONS AND DATA REDUCTION

Direct images of IC 4593 were obtained on May 17 1993 and May 1–3 1994, with the 2.1-m f/7.5 telescope of the Observatorio Astronómico Nacional at San Pedro Mártir, B.C., México. A Thomson TH31156 1024×1024 Metachrome II coated CCD detector was used in both runs. Plate scale was 0.25″/pixel, and image quality, measured by the FWHM of stars, was ∼ 1.5″. Sky exposures were secured for flat fields. The Hβ and [O III] 5007 frames are from the May 1993 run, where low level static noise appeared in the detector. A detailed log of these observations, including the filters' properties for an operating temperature of 0°C, is given in Table 1. Total exposure times are given in this table. For each filter we carried out a series of exposures, the longest ones for 20 minutes. None of them was saturated. A 5×5 pixel median filter, roughly equivalent to image quality, was applied to all images. [O I] 6300 and [S III] 6312 are transmitted

TABLE 1

IMAGING LOG

Filter		Main Lines	Exposure Time (min)
λ_0 (Å)	$\Delta\lambda$ (Å)		
4280	38	Continuum	20
4365	10	[O III]	80
4871	49	Hβ	40
5008	8	[O III]	60
5881	32	He I	40
5954	36	Continuum	20
6253	51	Continuum	20
6309	45	[O I], [S III]	80
6564	11	Hα	25
6586	11	[N II]	60
6729	52	[S II]	40
6733	11	[S II]	60
9069	43	[S III]	40

TABLE 2

SPECTROSCOPIC RESULTS[a]

ID	$F_\lambda/F(\mathrm{H}\beta)$	$I_\lambda/I(\mathrm{H}\beta)$	ID	$F_\lambda/F(\mathrm{H}\beta)$	$I_\lambda/I(\mathrm{H}\beta)$
[O II] 3726	20.0	20.8	[Cl III] 5518	0.52	0.51
[O II] 3729	11.9	12.4	[Cl III] 5538	0.44	0.43
H13	2.49	2.59	[N II] 5755	0.16	0.16
[Ne III] 3869	25.2	26.1	He I 5876	14.9	14.5
[Ne III] 3968	8.90	9.19	O III 5696	0.40	0.39
Hϵ	14.1	14.2	[S III] 6313	0.88	0.85
He I 4026	2.46	2.54	[N II] 6548	3.13	2.99
Hδ	24.6	25.3	Hα	294	280
Hγ	44.6	45.5	C II 6578	0.31	0.30
[O III] 4363	1.75	1.79	[N II] 6584	9.93	9.48
He I 4471	4.47	4.55	[S II] 6717	0.59	0.56
N III 4634	0.41	0.42	[S II] 6731	0.86	0.82
N III 4641	0.41	0.42	He I 7065	4.93	4.66
N III 4642	0.34	0.34	[Ar III] 7136	12.2	11.5
C III 4648	0.52	0.53	He I 7281	1.03	0.97
O II 4649	0.36	0.36	[Ar III] 7750	2.60	2.43
C III 4651	0.47	0.47	P16	0.56	0.52
C IV 4659	0.35	0.35	P15	0.42	0.39
He II 4686	1.20	1.21	P14	0.69	0.64
Hβ	100	100	P13	0.86	0.79
He I 4922	1.41	1.41	P11	1.28	1.18
[O III] 4959	170	169	P10	1.76	1.62
[O III] 5007	508	505	[S III] 9069	20.1	18.5
He I 5016	2.25	2.24	...	...	...

[a] $F(\mathrm{H}\beta) = 1.28 \times 10^{-11}$ erg cm^{-2} s^{-1}, $C(\mathrm{H}\beta) = 0.06$, and $I(\mathrm{H}\beta) = 1.47 \times 10^{-11}$ erg cm^{-2} s^{-1}.

by the filter centered at 6309 Å. Spectroscopy shows that the latter is stronger in the central region (see below). Since there is no spectroscopic observation outside this region, it is impossible to know the relative importance of both lines throughout the nebula, though the contribution of the sulfur line can be estimated from the image for [S III] 9069. Images at 4280, 5954 and 6253 Å were used to subtract the continuum from frames including one or more emission line, with the exception of the one containing [S III] 9069. All continuum subtracted images were calibrated using our unreddened spectral results.

Due to differences in the point spread function, image subtraction is somewhat problematic at the stellar scale. Thus, some residual flux from the central star of IC 4593 is left when subtracting the continuum. Since the spectral diaphragm is relatively large (see below), we were able to sample these images sufficiently far from the region where effects introduced by continuum subtraction are important.

Thus, numerical results extracted from the flux calibrated Hα image are probably correct within 25%. Relative precision within any line ratio image can be estimated assuming that the main source of uncertainty is the sky background being subtracted from the source frames. Error images were produced in this fashion, and used to confine line ratio images so that the relative accuracy throughout them is better than 50%. Precision in the brightest regions is better than this. Data reduction was carried out with IRAF[2].

The object was observed on May 18–21 1994, with the REOSC echelle spectrograph and the same telescope and detector. The spectral setup consisted of a 300 lines mm^{-1} grating, a 300 μm wide slit aligned in the NS direction, a 1-mm long mask (corresponding to 13.5$''$), and a He-Ar comparison lamp. All

spectra were centered at the position of the central star. Four spectra were obtained in order to cover the optical domain: 3450–5800 Å, 4790–7110 Å, 6300–8480 Å and 7590–9180 Å. Given the spectral setup we missed some important lines, in particular He I 6678 and [O II] 7325. Spectral dispersion varied from 0.09 Å/pixel at the blue end, to 0.28 Å/pixel in the red. The spectral resolution is ~ 3 pixel at 4650 Å. Total exposure times were 30 minutes for the first three spectra, and 40 minutes for the last one. Flux calibration was carried out with standard stars Hz44 and BD+33 2642. IRAF standard procedures were used for data reduction.

3. SPECTROSCOPY

Results are shown in Table 2. As can be seen from the Balmer ratios, extinction in IC 4593 is very small. Assuming case B Balmer decrement with $H\alpha/H\beta = 2.8$, and Whitford's extinction law as given by Miller & Mathews (1972), we obtain $C(H\beta) = 0.06$. Very similar values, ranging from 0.06 to 0.08, have been derived by others (Peimbert & Torres-Peimbert 1971; Kaler 1976; Le Van & Rudy 1983). Line intensity errors were estimated comparing fluxes from lines present in more than one of the overlapping spectra. For the most intense lines the error is less than 10%, whereas in the weakest lines, such as [N II] 5755, and lines redward of 7600 Å, where flux calibration suffered from poor signal from the standard star, it can be as large as 30%, as can be seen when comparing the observed Paschen line intensities with theoretical expectations. Barker (1978) reports the existence of [S II] 4072. Neither us nor Czyzak et al. (1975) detected these lines. On the other hand, Czyzak et al. (1975) cannot resolve [O I] 6300 from [S III] 6312. After deblending, they conclude that [O I] 6300 is 3.7 times brighter. This is probably incorrect, since we detected [S III] 6312 but no significant [O I] emission in the central region. [O I] 6300 is at the edge of the free spectral range, but [O I] 6364 is well within it, and we found it to be ≤ 0.09 ($H\beta = 100$). We have a positive, albeit very weak, detection for He II, which was not found by either group.

A 40 minutes *IUE* short wavelength spectra of the nebula (SWP 31291) is available. Only two features are evident in the nebular spectrum, $L\alpha$ and the N III] complex at 1748 Å, whose fluxes are 7.3×10^{-12} and 5.6×10^{-13} erg cm^{-2} s^{-1} respectively. There is a weak line which might be C III] 1909, but the identification is very uncertain (the line center is at 1903 Å) and the intensity barely above the noise level. Otherwise, there is no other feature in the UV spectrum of the nebula. In particular, the absence of He II 1640 Å complicates the calibration procedure. Using Seaton's (1979) extinction law with $C(H\beta) = 0.06$, the unred-

dened fluxes for $L\alpha$ and N III] 1748 are 1.1×10^{-11} and 7.5×10^{-13} erg cm^{-2} s^{-1} respectively. In order to obtain a ratio for N III] 1748/Hβ, we used the flux calibrated Hα image (see next section) to derive the Hβ flux over the diaphragm used by the *IUE* (large aperture mode, $10.5'' \times 21''$), centered at the position of the central star with the corresponding position angle of the *IUE* (PA = 24.48°). For this diaphragm, $I(H\beta) = 2.8 \times 10^{-11}$ erg cm^{-2} s^{-1}, so that N III] 1748/Hβ = 0.0265.

According to Dinerstein (1980), the flux of [S IV]10.5 μm, over a 10'' circular diaphragm centered on the Planetary Nebula Nucleus (PNN), is 1.4×10^{-11} erg cm^{-2} s^{-1}. From the flux calibrated Hα image we obtain $I(H\beta) = 2.2 \times 10^{-11}$ erg cm^{-2} s^{-1} with the same diaphragm. This leads to [S IV]10.5 μm/Hβ = 0.64.

Densities and temperatures derived from different forbidden line ratios are shown in Table 3, where we also include sources used to obtain these quantities. Spectral regions including some of these lines are shown in Figure 1. The x parameter derived from low ionization species, O$^+$ and S$^+$, is twice as large as the value found from the Cl^{+2} ratio. This difference indicates that the low excitation gas resides in denser regions. Temperatures (t, in 10^4 K) obtained from [N II] 6584/5755 and [S III] 9069/6312 are 16 and 7% higher than the one derived from [O III] 5007/4363. These differences are not large, and to a large extent they are due to observational errors. As can be seen in Fig. 1, [N II] 5755 is quite weak and it may well have been overestimated, leading to an artificially large value for the temperature. On the other hand, the S^{+2} lines are intense but, as mentioned before, flux calibration at the red end of the spectrum is not particularly good. Finally, [O III] 4363 is very well determined, and errors in the O^{+2} ratio do not exceed the 15% level, which leads to a 300 K uncertainty in the temperature. Thus, the O^{+2} temperature is adopted to calculate all ion concentrations.

TABLE 3

PHYSICAL PARAMETERS

	Ratio	x	t	N_e	Refs.[a]
[O II] 3726/3729	1.68	0.26	0.84	2800	1
[S II] 6717/6731	0.68	0.26	0.84	2800	1
[Cl III] 5518/5538	1.18	0.13	0.84	1400	2
[O III] 5007/4363	282	...	0.84	...	1
[N II] 6584/5755	59	...	0.99	...	1
[S III] 9069/6312	22	...	0.91	...	3

[a] References. (1) McCall 1984; (2) Torres-Peimbert & Peña 1991; (3) Aller 1984.
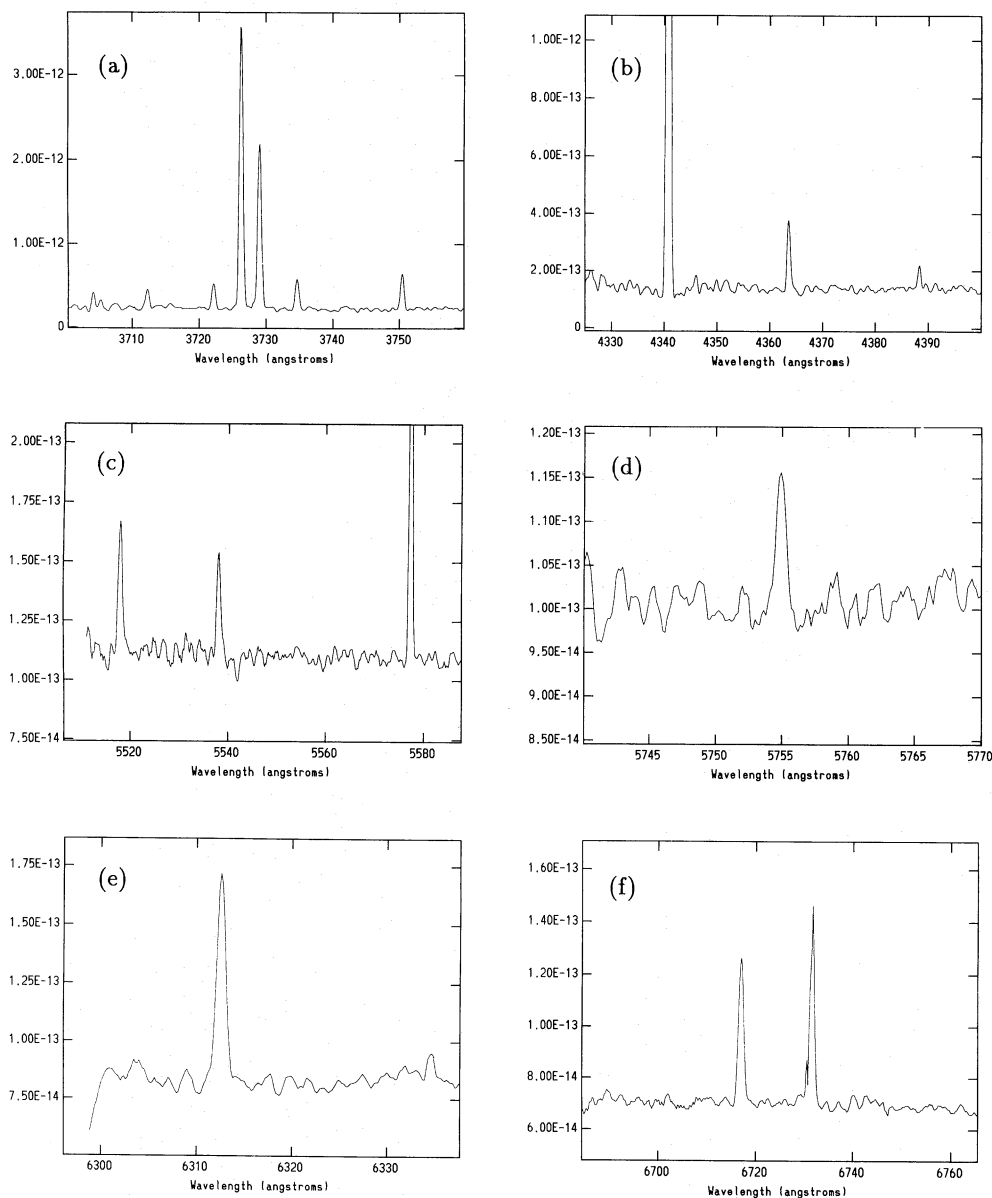
Fig. 1. Spectrum of IC 4593 around (*a*) the O$^+$ lines at 3726, 3729 Å; (*b*) the O^{+2} line at 4363 Å; (*c*) the Cl^{+2} lines at 5518, 5538 Å; (*d*) the N$^+$ line at 5755 Å; (*e*) the S^{+2} line at 6312 Åand (*f*) the S$^+$ lines at 6717, 6731 Å.

Ion abundances are reported in Table 4. Aller's (1984) formulae were used for the helium abundances as found from the He I 4471, He I 5876 and He II 4686 lines. The work of Torres-Peimbert & Peña (1991) was used to find the He$^+$ abundance from the He I 4922 line. Collisional correction factors for helium (Clegg 1987) are very small ($\leq$ 5%), and were not deemed necessary. The abundance of S^{+2} obtained from the 9069 Å line was calculated follow-

ing Aller (1984). The emissivity for [S IV] 10.5 μm was determined from a program developed by S. Adams and I. Howard at UCL, England (kindly made available by R. Kingsburgh). For the aforementioned temperature and density, K([S IV] 10.5 μm) = 3.3 $\times$ 10^{-6}. All other ion concentrations were calculated from Torres-Peimbert & Peña (1991).

Elemental abundances are also shown in Table 4. We used the ionization correction factors (ICF) of

Kingsburgh & Barlow (1994). Abundances for non-type I planetary nebulae, as given by these authors, are included for comparison. Nitrogen abundance was calculated in two ways: using only the optical data and applying the corresponding ICF, and, secondly, adding all ion concentrations using the UV information. In the first case the calculated nitrogen abundance is 3×10^{-5}, in the second we derive 1.7×10^{-4}. Thus, either the ICF is way off, and/or the operations leading to the abundance of N^{+2} from the UV data are plagued with errors. We did the same for the abundance of sulfur, using the IR information. Slightly larger abundances are derived when the IR data is used (e.g., 4.3 instead of 4.9×10^{-6} when using the [S III] 9069 line), but these differences are not significant. The determination of the C^{+2} abundance from C III 4648,4651 depends on whether case A or case B is prevalent for the carbon recombination lines. Kaler (1976) suggests that case A is more adequate. French (1983) derives C^{+2}

abundances based on this assumption. We annotate the concentration of C^{+2} derived from each of these cases in Table 4. Total carbon abundance is only given for case A.

Abundances determined in this work are generally larger than previous estimates. Furthermore, as can be seen from Table 4, most abundances in IC 4593 are typical of non-type I planetaries. Neon might be slightly underabundant, but our determination is based in only one ionization stage. Optical data alone would imply that nitrogen is underabundant with respect to this sample, but the UV data leads to a normal value. Further research would be required to elucidate the origin of this discrepancy. Case A total carbon abundance is also found to be normal, but almost 2 times less than French (1983) estimate. According to French (1983), carbon exists mostly as C^{+3}. The absence of C IV 1550 in the UV spectrum, from where we find that $C^{+3}/H^+ \leq 9.2 \times 10^{-7}$, indicates that this is not so. On the other hand, C II 4267 was not detected by Czyzak et al. (1975) nor us. All this would imply that most of carbon is C^{+2}, were it not for our detection of C II 6578, for which we could not find atomic data to calculate the ion concentration. An additional warning regarding the carbon abundance, is that the C III 4648, 4651 lines are weak, blended and variable (at a $\sim 4\%$ level), with possibly a significant stellar contribution (Méndez et al. 1990). Finally, the detection of Lα in the UV spectrum poses a problem on the legitimacy of assuming case B recombination and, consequently, on the abundance determinations. Our conclusions

TABLE 4

ABUNDANCES

| Ion	Line	X^{+i}/H^+
He$^+$	4922	0.105
...	4471	0.091
...	5876	0.103
He^{+2}	4686	0.001
O$^+$	3726, 3729	4.1×10^{-5}
O^{+2}	5007	3.2×10^{-4}
N$^+$	6584	3.1×10^{-6}
N^{+2}	1748	1.7×10^{-4}
C^{+2} (case A)	4648, 4651	8.3×10^{-4}
C^{+2} (case B)	...	1.2×10^{-4}
S$^+$	6716, 6731	6.9×10^{-8}
S^{+2}	6312	3.4×10^{-6}
...	9069	2.8×10^{-6}
S^{+3}	10.5 mμ	2.1×10^{-6}
Ne^{+2}	3869	5.8×10^{-5}
Ar^{+2}	7136	1.6×10^{-6}
Cl^{+2}	5518, 5538	1.2×10^{-7}
Element	IC 4593	non-Type I[a]
He	0.104	0.112 ± 0.015
O	3.6×10^{-4}	$5.2 \pm 1.7 \times 10^{-4}$
N	0.3–1.7×10^{-4}	$2.5 \pm 1.5 \times 10^{-4}$
C (case A)	9.3×10^{-4}	$8.1 \pm 4.9 \times 10^{-4}$
S	4.3–5.5×10^{-6}	$1.0 \pm 0.6 \times 10^{-5}$
Ne	6.6×10^{-5}	$1.3 \pm 0.4 \times 10^{-4}$
Ar	3.0×10^{-6}	$3.0 \pm 1.8 \times 10^{-6}$

[a] From Kingsburgh & Barlow 1994.
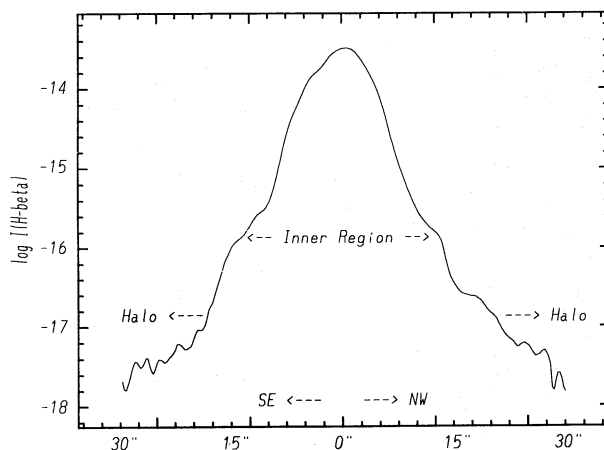
Fig. 2. Scan for the log Hβ image along the axis defined by the ansae. The SE and NW labels mark the directions towards the southern and northern ansae. The limits defining the outer boundary of the inner region and the inner boundary of the halo are also shown. Obviously, the intermediate region lies between these two.

hold if Lα is predominantly produced in the stellar wind, but if this is not so, case B recombination is not fully applicable.

4. IMAGING

In order to investigate if there are significant extinction inhomogeneities, we inspected the Hα/Hβ image ratio, and found that variations around the mean value are not larger than 15%. This implies that extinction is quite uniform —and fairly small— throughout IC 4593. Imaging analysis will be based in the Hα image, for which we have a better signal. As mentioned previously, the Hα image was calibrated using the unreddened flux derived from

our spectroscopic observations. To ease comparisons with the spectroscopic data, the flux calibrated Hα image was divided by 2.8 to produce a pseudo Hβ image. Henceforth we will refer to it as the Hβ image. All other frames are with respect to it, and were calibrated using the unreddened spectral data. Given the fact that extinction is relatively uniform and small, this procedure is acceptable.

A scan across the continuum subtracted Hβ image along the axis defined by the ansae (PA $= 135°$) is displayed in Figure 2. The scan extends $30''$ on either side of the PNN. We used a logarithmic scale. As can be seen, surface brightness in the faintest regions is $\sim 3 \times 10^4$ times smaller than in the brightest spot (I_{max}). In order to render all nebular features, the
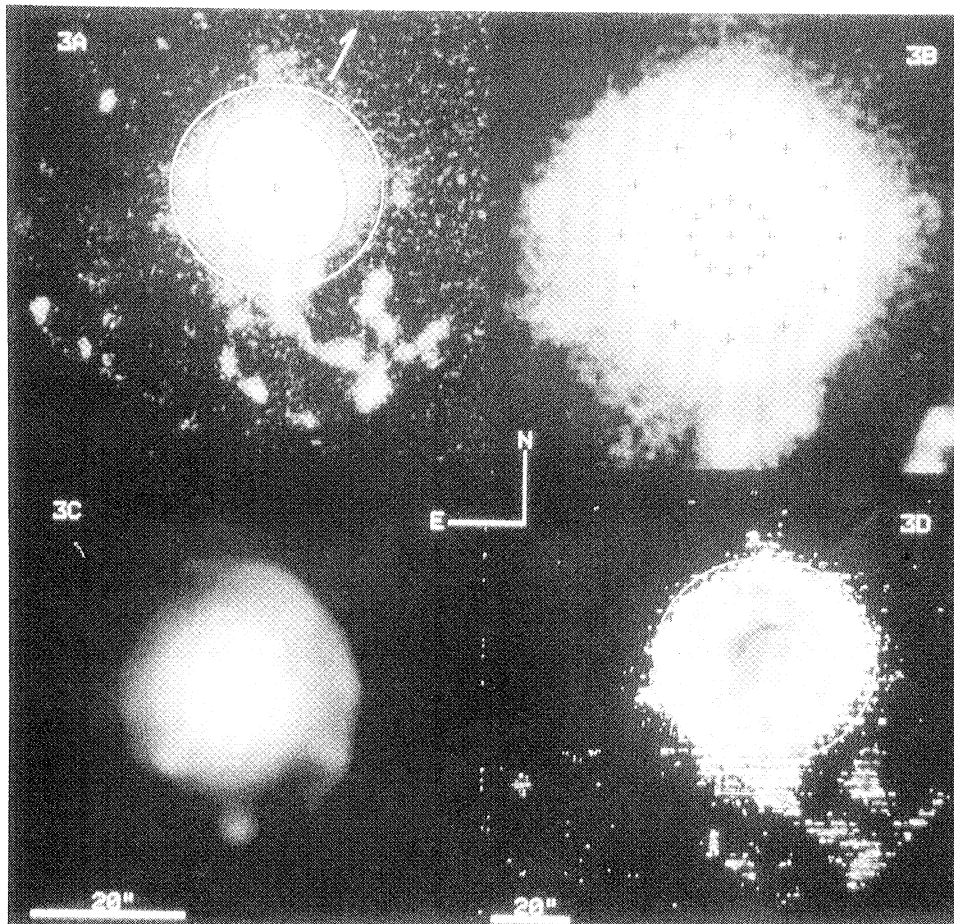

Fig. 3. Frames (a), (b) and (c) are the continuum subtracted Hβ image displayed in different intensity ranges with a logarithmic scale. Frame (d) is the [O III] 5007/Hβ line ratio image. Plate scale for frames (a) and (d) is presented at the bottom of frame (d), and the one for images (b) and (c) appears at the bottom of frame (c). The position of the PNN is marked with a "+" sign in Figs. 3a and 3b. Positions for the data points presented in Figs. 4 and 5, are marked in Fig. 3b. The direction of the proper motion vector is presented in Fig. 3a. A $28''$ circle centered at the position of the PNN is drawn in Figs. 3a and 3d. The ellipse drawn in Fig. 3a is with the parameters given in section 4.2.

continuum subtracted Hβ image is displayed in Figures 3a, 3b and 3c in three different intensity ranges. We zoomed into the nebula (by a factor of 2) in Figs. 3b and 3c. Differences in excitation across the nebula can be seen in Fig. 3d, where an image for the [O III] 5007/Hβ ratio is displayed with the normal spatial scale. Various components can be identified from the information conveyed by these frames: (i) a nearly circular inner region, best seen in Fig. 3c, (ii) beyond it, an elliptical structure with a prominent arc towards the NW, (iii) a circular and irregular halo surrounding the latter and (iv) the inner ansae and a number of condensations, most of them towards the SW and beyond the halo. In the following subsections we describe each of these separately.

4.1. Inner Region

The Hβ flux decreases very rapidly up to $\simeq 10''$ from the central star (see Fig. 2). Within this region, surface brightness is $\geq I_{max}/200$. This level approximately defines a nearly circular region and the two protruding ansae. Line ratio images, in particular [O III] 5007/Hβ (see Fig. 3d), reveal numerous structural details and a large scale azimuthal asymmetry within the inner nebula. Line intensities for [O III] 5007, [N II] 6584 and He I 5876 with respect to Hβ are smaller in the NE half, particularly along an arc running eastwards from the northern to the southern ansa, located between 7'' and 9'' away from the central star. Along this arc [O III] 5007/H$\beta \leq 3$, with the smallest value ($\simeq 1.8$)
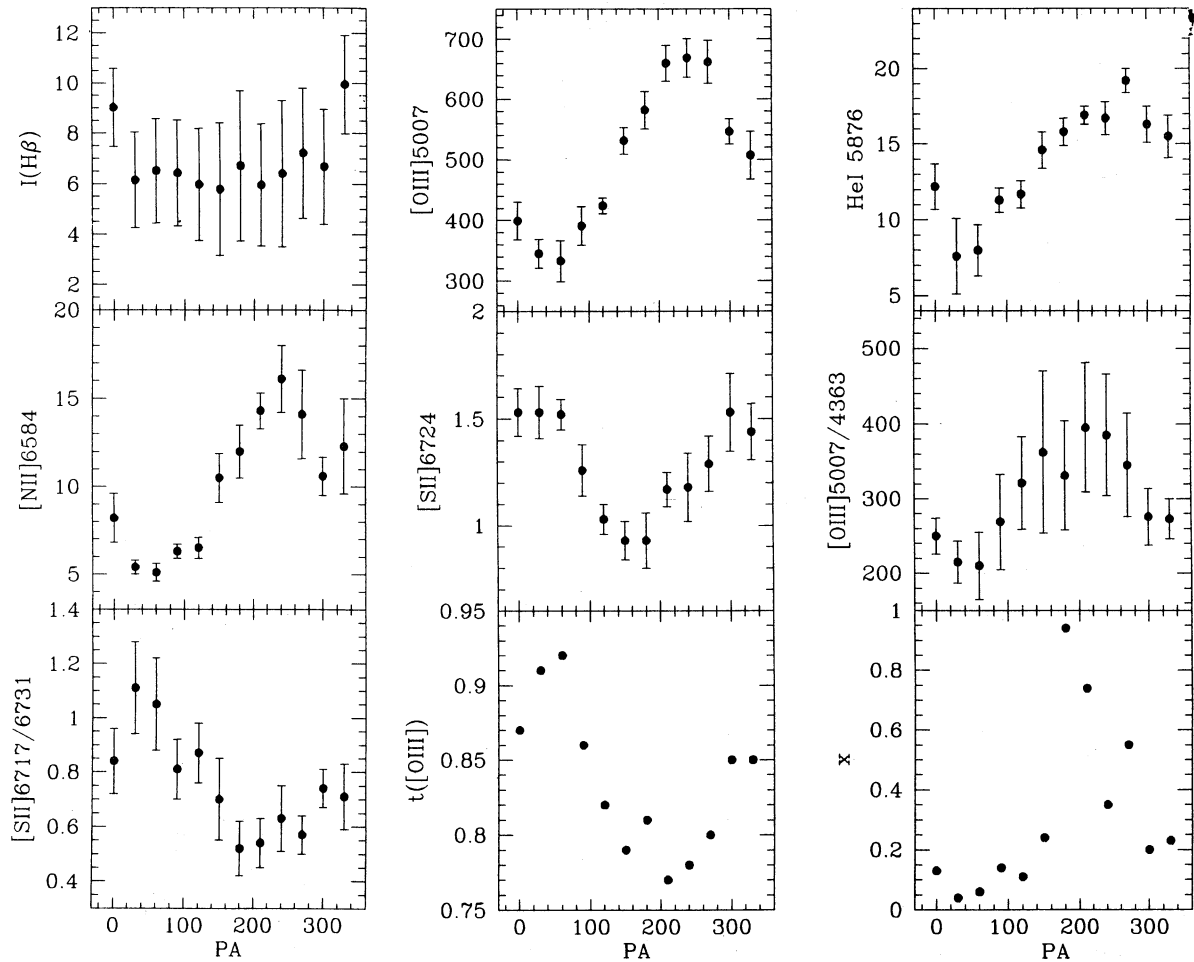

Fig. 4. Azimuthal scans for (a) I(Hβ), (b) [O III] 5007/Hβ, (c) He I 5876/Hβ, (d) [N II] 6584/Hβ, (e) [S II] 6724/Hβ, (f) [O III] 5007/4363, (g) [S II] 6717/6731, (h) t([O III]) and (i) x. All scans run counterclockwise from PA = 0°. As a reference, the southern and northern ansae are located at PA = 135° and PA = 315°. Each data point is 5'' distant from the PNN. A 2.25'' × 2.25'' diaphragm was used. The Hβ flux is given in 10^{-13} erg cm^{-2} s^{-1}. In this representation Hβ = 100 and Hα/Hβ = 2.8. The temperature (t([O III]) and the x parameter were calculated from the mean values for [O III] 5007/4363 and [S II] 6717/6731.

some 3.5″ to the NW of the "Hα blob" described by Zucker & Soker (1993) (see Fig. 3c). At the position of the "blob", with a 9 × 9 pixel diaphragm (2.25″ × 2.25″), $I(H\beta) \simeq 8.4 \times 10^{-13}$ erg cm^{-2} s^{-1} and $N_e \simeq 3200$ cm^{-3}.

We inspected the azimuthal distribution of various quantities in a ring 5″ distant from the central star (where there is no effect from continuum subtraction and we have information on all lines), using the aforementioned diaphragm. Plots of these quantities as a function of the azimuthal angle, measured counterclockwise from PA = 0° with 30° steps between each pair, are presented in Figure 4. Positions for these data points are marked with a "+" sign in Fig. 3b. As a reference, the position angles of the southern and northern ansae are 135° and 315° respectively. An outstanding feature in Fig. 4 is that all line ratios display a regular pattern of variations as a function of the position angle. With the exception of [S II] 6724/Hβ, the same pattern is observed in all line ratios. The Hβ flux has a well defined peak to the north, in the direction of the "Hα blob", but is quite uniform throughout the rest of the ring. This is not the case for the line ratios. Those involving [O III] 5007, He I 5876 and [N II] 6584 have a minimum at PA ≃ 60°, and a maximum at PA ≃ 240°, whereas [S II] 6724/Hβ has a clearly defined minimum in the direction of the southern ansa. Density and temperature distributions in the ring, as evinced by [S II] 6717/6731 and [O III] 5007/4363, are also variable. The largest density, ≃ 8500 cm^{-3}, is found in the SE quadrant at PA = 150°, and the minimun value, ≃ 400 cm^{-3}, at PA = 0°. Temperature variations run oppositely to the density distribution: the smallest temperature (7700 K) occurs near the position of maximum density, and the largest value (9200 K) is found around the region where the density is smaller.

Ion concentrations in the ring were roughly estimated from the preceding data and the work of Torres-Peimbert & Peña (1991). We find that the concentration of all ions is inhomogeneous, being consistently larger in the NW (PA ≃ 270°) than in the SE (PA ≃ 60° − 90°). The differences can be very large, up to a factor between 2 and 6. Such large differences are probably artificial, as they are introduced by the number of operations involved in the calculation of abundances. Nevertheless, all parameters consistently indicate that the density, temperature and excitation in the inner nebula are very inhomogeneous. These variations are not random, but have a clearly defined azimuthal distribution. This conclusion is totally different to the assumption advanced by Czyzak et al. (1975). Quite obviously, spectroscopy with a smaller diaphragm and careful positioning would produce more accurate information on the extent of these inhomogeneities.

From the flux calibrated image we obtain $I(H\beta)$

$\simeq 3.0 \times 10^{-11}$ erg cm^{-2} s^{-1} for the inner region and 3.1×10^{-11} erg cm^{-2} s^{-1} for the entire nebula. Thus, most of the mass of ionized gas is located within the inner region. The mass of ionized hydrogen can be found from

$$M(H^+) = \frac{4\pi D^2 m_H I(H\beta)}{E_{42} N_e} \ , \qquad (1)$$

where D is the distance to the object, m_H the proton mass, E_{42} the effective recombination emissivity and N_e the electron density. Since the extent of the density map where information is sufficiently reliable is more limited, we take the density to be uniform and equal to the one derived from our spectroscopic observation (Table 3). For the inner nebula we find that $M(H^+) \simeq 0.53(D_{kpc}/4.3)^2 \ M_\odot$, where D_{kpc} is the distance to IC 4593 in kiloparsec. Considering the helium abundance, as given by the spectroscopic data, the ionized gas mass in the inner nebula is $\simeq 0.72(D_{kpc}/4.3)^2 \ M_\odot$. Other mass estimates yield 0.4 $M_\odot$ (Phillips & Pottasch 1984) and 0.3 $M_\odot$ (Zucker & Socker 1993) within 6″ of the central star, for a distance of 4.3 kpc to the object. According to Méndez et al. (1990), the mass of the central star is $0.74 \pm 0.06 \ M_\odot$. If we are measuring all the nebular mass, the progenitor's mass was ∼ 1.5 $M_\odot$. All mass estimates are upper limits to the real value, since we are assuming that the filling factor is unity.

4.2. Intermediate Region

This region is located roughly between 10″ and 20″ from the central star. It is obviously detached from the inner region and is structurally different from the surrounding halo (see Fig. 3b). The intermediate region is probably shaped by gas dynamical processess, whereas the halo is clumpy. Furthermore, the halo is much more highly excited (Fig. 3d). The surface brightness of Hβ at the outer boundary is $\geq I_{max}/2000$. This level defines an almost perfect ellipse (Fig. 3a) with the following parameters: a = 21″, b = 18″, e = 0.53 and PA = 31.7° (major axis). Thus, the major axis of the ellipse is almost perpendicular to the axis defined by the ansae, where PA = 135°. The outer boundary is particularly well defined in the northwestern quadrant, where contrast with the surrounding halo, in terms of the Hβ flux and the [O III] 5007/Hβ line ratio, is very conspicuous. On the other hand, the eastern outer boundary is not as prominent in terms of the Hβ flux, and very diffuse insofar as the [O III] 5007/Hβ line ratio is concerned.

As with the inner nebula, we explored the azimuthal distribution of some physical quantities in the intermediate region. Results for $I(H\beta)$ and [O III] 5007/Hβ, the only quantities for which we have reliable data, are presented in Figure 5.
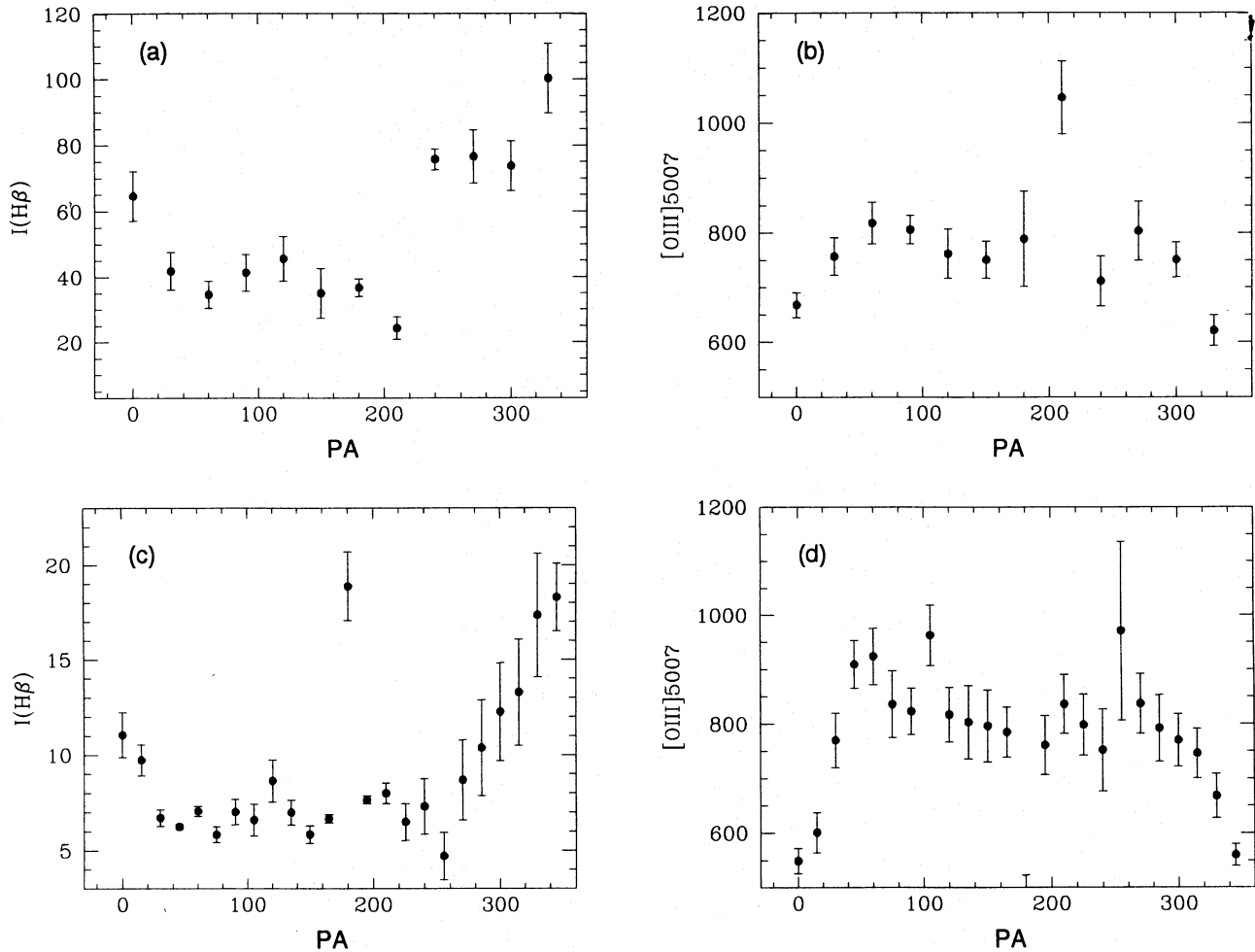
Fig. 5. Azimuthal scans for (a) $I(H\beta)$ and (b) [O III] 5007/$H\beta$ carried out along a circle 14″ away from the PNN, and the same parameters as in Fig. 4. Positions of data points are marked in Fig. 3b. Figures (c) and (d) are for the same quantities, but the diaphragm was positioned just within the ellipse displayed in Fig. 3a. (a = 19″, b = 16″). In this case the diaphragm is smaller (1.25″ × 1.25″), and data were sampled every 15°. The $H\beta$ flux is given in 10^{-16} erg cm^{-2} s^{-1}.

Measurements in Figs. 5a and 5b were made in the same directions and with the same diaphragm (2.25″ × 2.25″) as in the inner region (Fig. 4), but the ring is 14″ distant from the central star. Positions are marked in Fig. 3b. In Figs. 5c and 5d we positioned the diaphragms (in this case 1.25″ × 1.25″) along an ellipse immediately inside to the one defining the outer boundary of the intermediate region. The same general behaviour is observed in both configurations. $I(H\beta)$ is roughly constant towards the south and southeast (the peak at PA = 180° is from a condensation) and, as expected, enhanced in the NW direction. The distribution is not unlike the one found in the inner region, though the area where $H\beta$ emission is enhanced is spread out over a larger angle (∼ 120°, as opposed to ∼ 60° in the inner re-

gion). The contrast between the SE and NW halves is twice as large in the intermediate than in the inner region. On the other hand, the [O III] 5007/$H\beta$ line ratio reveals that the excitation level in the intermediate region is higher. [O III] 5007/$H\beta$ is obviously smaller towards the north, otherwise it is fairly constant. Thus, as opposed to the inner region, no regular pattern of azimuthal variations is observed in this case.

4.3. Halo

The halo extends up to ∼ 30″ [$0.5(D_{kpc}/4.3)$ pc] from the central star. The outer boundary is irregular but approximately spherical, and centered at the position of the PNN (see the circles drawn in Figs. 3a

and 3d). Given the large extension of the intermediate region, particularly in the NE-SW axis, the halo occupies a comparatively small fraction of the volume of IC 4593. In absolute terms it is as extended as the halos of other planetaries. Some irregularities in the outer boundary are probably related to small condensations. For instance, the halo is less extended towards the SW, where there is a string of condensations beyond it. It is questionable whether this is the reason why it is slightly more extended in the NW and SE quadrants (which have the same extension) than in the other two. The halo has the clumpy structure usually associated to H II regions, but also found in the halos of other planetary nebulae. As is apparent from Fig. 3d, it is the most highly excited region in IC 4593, with [O III]/Hβ $\simeq$ 15, though there are quite a few randomly distributed structures departing from the mean. Highly excited halos have been found in other planetaries, such as NGC 6826 (Phillips & Reay 1983) and NGC 7009 (Bohigas, López, & Aguilar 1994), and are explained in terms of radiation hardening (Aller et al. 1980). The structure, degree of excitation and irregularities observed in the halo imply that it is real, not merely stray light, which would hardly produce the effects mentioned above. Thus, the halo is not overly extended in any direction, and there is no morphological or spectroscopic peculiarity in any region within it. In particular, we find no evidence for a "bump" in the NW edge of the nebula. This structure is described by Zucker & Socker (1993), who propose that it is formed by a Rayleigh-Taylor instability at the edge of a shock front. We suggest that this discrepancy may be due to the fact that we used narrower filters (Table 1) and subtracted the continuum, which can be significant in these low surface brightness regions. If our conclusion holds, it weights against the hypothesis that the shaping of the NW boundary of IC 4593 is due to supersonic expansion into the ISM.

4.4. Ansae and Condensations

The ansae are symmetrically disposed at an angular distance of 13″ from the central star [0.25$(D_{kpc}/4.3)$ pc]. Spectral information on the ansae, derived from the calibrated image ratios, is annotated in Table 5. In this case we used a 7 × 7 pixel diaphragm (1.75″ × 1.75″), which roughly corresponds to their angular diameter. The most salient feature is that emission from low excitation lines is comparatively stronger in the ansae. From the flux for [S III] 9069, and assuming that [S III] 9069/6312 = 20, we conclude that, at the ansae, $\simeq$ 70% of the light transmitted by the filter centered at 6309 Å is from [O I] 6300. Notice that the mass for the ansae (obtained for t = 0.84) is some 5 times smaller than the one derived by Zucker & Socker (1993). We think that our result is more reliable, since it was ob-

TABLE 5

ANSAE PROPERTIES

	NA	SA
Hβ	100	100
[O III] 5007	544±43	518±39
He I 5876	18.8±2.5	18.2±2.5
[O I] 6300, [S III] 6312	4.7±0.8	2.6±0.8
[N II] 6584	54.0±10.5	64.0±7.6
[S II] 6724	8.1±1.0	6.1±1.2
[S III] 9069	14.2±2.6	10.7±3.8
[S II] 6717/6731	0.59±0.15	0.79±0.24
x	0.47	0.16
$F(H\beta)$ $(10^{-14}$ erg cm^{-2} s$^{-1})$	1.0±0.2	0.7±0.1
M(H$^+$) $[(D_{kpc}/4.3)^2$ $M_\odot]$	2.9×10^{-5}	5.9×10^{-5}

tained from a direct measurement of the density. In the framework of Soker's (1992) model for the production of jets, this would imply that the ansae are fast jets produced after the AGB phase.

Beyond the inner region there is a large number of condensations, the majority located to the SW and beyond the halo. The most distant condensation is 72″ to the SE of the central star [$\simeq$ 1.3$(D_{kpc}/4.3)$ pc]. Most condensations group to form three separate and well defined strings, though a few of them are either isolated or detached. Two of these strings are connected to the main body of the planetary. All these structures are concave towards the NW, as opposed to the presumed bow shock at the NW edge of the intermediate region. Their arrangement suggests bursts of activity in a precessing source, the same kind of picture that was advanced for the planetary nebulae NGC 6543 and Fg 1 (Miranda & Solf 1992; López, Roth, & Tapia 1993). In fact, were it not for the absence of a similar set of structures at the opposite side of the nebula, a single string of condensations in IC 4593 would bear a striking resemblance with the string of knots discovered in Fg 1 (López et al. 1993), which also displays a "twisted arm" morphology. The neat spatial arrangement of the knots in Fg 1 immediately suggests a series of episodic mass ejection events. A reconstruction of a similar series of events in IC 4593 is far more difficult, since there are three contiguous strings composed of knots with similar surface brightness, with no counterpart at the opposite side of the PNN.

The asymmetrical disposition of these condensations is puzzling. Zucker & Socker (1993) have suggested that the condensations might have been produced in the wake of the bow shock wave revealed by the NW arc of the intermediate region. But this pro-

cess would generate a similar set of condensations on the either side of the PNN, and not predominantly in the SW quadrant. Notice also that some condensations are located at the opposite side of the NW arc, on the "shadow" of the shock front. Thus, the orientation, arrangement and overall distribution of the condensations does not seem amenable to this scenario. It would be tempting to suggest that the supersonic expansion of IC 4593 into the ISM destroyed the NE set of condensations, but we have the same objections to this hypothesis. It is also conceivable that the condensations were produced by a series of ejections from the PNN, and that some structure or process prevented (or favoured) their ejection in one direction and, at the same time, generated the observed asymmetries in the inner and intermediate regions.

The condensations are characterized by comparatively large values for [S II] $6724/H\beta$: from 0.2 to 0.4, some 20 times higher than in the inner nebula. Correcting for the abundance difference, we find that these values can be explained with a radiative bow shock wave model (Hartigan, Raymond, & Hartmann 1987). However, this is not the case for [O III] 5007, which is too strong to be accounted for in this type of model. Values for [O III] $5007/H\beta$ are similar to those found in parts of the inner nebula ($\simeq$ 3–4), as had been noticed by Zucker & Socker (1993). Even though we took a very long exposure, just one very faint condensation is visible in the frame centered at 6300 Å, which implies that these are not neutral. Density information is restricted to three of the brightest condensations, where we find $x \simeq$ 0.90, 0.97 and 0.96. These crude results are surprisingly uniform, and suggest the existence of a high density core. For all the condensations we obtain $I(H\beta) \simeq 1.3 \times 10^{-13}$ erg cm^{-2} s^{-1}. If the mean density is $\geq$ 1000 cm^{-3}, the total H$^+$ mass in this component is $\leq 1.9 \, (D_{kpc}/4.3)^2 \times 10^{-3} \, M_\odot$.

5. IS THERE A BOW SHOCK?

As mentioned, it has been suggested that the intermediate region is shaped by the supersonic expansion of IC 4593 into the surrounding ISM (Balick et al. 1992; Zucker & Socker 1993). The contention is supported by the contrast between the NW and SE quadrants, which recalls the structure of a bow shock, and, more strongly, by the direction of the proper motion vector. The position angle of the latter is $335^{+15°}_{-20}$ (not $\sim$ 290°, as given by Zucker & Socker 1993), and is displayed in Fig. 3a. It is in the general direction of the normal to the surface of the NW arc, but far from perpendicular to the surface of the "blob", as was portrayed in Figure 2 of Zucker & Socker (1993). From the observational standpoint we find this model inconclusive. First, we notice that this region is confined by the halo, which does not

display any particular feature that would indicate it is subject to the effects of a shock wave. Furthermore, the system of condensations, above all their lopsided distribution, is hard to reconcile with this model. We also observe that the azimuthal distribution of $I(H\beta)$ in the inner and intermediate regions of IC 4593, is qualitatively the same. Since we do not expect the interaction with the ISM to be determinant for the inner region, we suspect that this shared property may be caused by a process inherent to the planetary. On the other hand, this argument is disfavoured by the very different azimuthal distribution of [O III] $5007/H\beta$ in these two regions. Finally, shocks tend to enhance ratios of forbidden to recombination lines. The opposite situation occurs in the NW arc: both [O III] $5007/H\beta$ and [S II] $6724/H\beta$ (see Fig. 3a of Zucker & Socker 1993) are smaller along it.

The kinematic properties of IC 4593 do indicate that it is moving supersonically, as long as the temperature in the surrounding ISM is $\simeq 10^4$ K. But the nebula is also being supplied with energy from the central star, amongst other things by its wind. The shaping of IC 4593 will be essentially determined by whichever source is furnishing more energy. The shock wave will be dynamically significant if its ram pressure is larger than the ram pressure of the wind of the central star, that is, if

$$\rho_0 V^2 \geq \frac{\dot{M}_w V_w}{4\pi R^2} \, , \qquad (2)$$

where ρ_0 is the pre-shock mass density, V the shock velocity (140 km s^{-1}, Zucker & Socker 1993), $\dot{M}_w$ and V_w the mass loss rate and wind velocity ($4 \times 10^{-8} \, M_\odot$ yr^{-1} and 1400 km s^{-1}, Hutsemekers & Surdej 1989; Cerruti-Sola & Perinotto 1989), and R the distance from the planetary to the NW arc $[0.4/(D_{kpc}/4.3) \, pc]$. Thus, the shock will be dynamically important if $n_0 \geq 0.06 \, (D_{kpc}/4.3)^2$ cm^{-3}, where n_0 g is the pre-shock particle density. At the minimum possible height above the plane for IC 4593 (1 kpc, Amnuel et al. 1984), the latter value is too high for the expected density of the warm component of the interstellar medium at this distance from the plane (Bohigas 1988; Reynolds 1991). Much more so at 2.8 kpc, the height that is derived from Cudworth's (1974) distance determination (which, by the way, is found from the same data used to derive the proper motion of IC 4593). If IC 4593 were expanding into the hot component, the situation would be worse. This density can be achieved if there were an anomalous density enhancement in the vicinity of the planetary. Consequently, it is likely that just the wind of the central star is more significant in determining the dynamical behaviour of IC 4593.

If this indeed the case, it would remain to develop

an alternative scenario that could account for the observed asymmetries in the inner and intermediate regions, the lopsided distribution of the system of condensations and the gross misalignment between the major axis of the ellipse defining the intermediate region and the line connecting the inner ansae. A small scale structure, such as the one reported by Zucker & Socker (1993), with a peculiar geometrical disposition, might be at the heart of it. It could redirect episodic mass loss events and generate the observed asymmetries in line intensities. The notion is vague, and the program intimidating, but planetaries can be very complex objects.

6. CONCLUSIONS

1. Compared with previous works, we obtain higher abundances for all inspected elements. The abundances of helium, oxygen, carbon, sulfur and argon in IC 4593 are typical of non-type I planetary nebulae. Neon abundance is somewhat less than the mean value for this type of planetaries, but this result is questionable since we have information of only one ionization stage (Ne^{+2}). Optical data alone leads to nitrogen underabundance by a factor of 3, but the abundance is found to be normal when UV information is used. This large discrepancy may be due to an inappropriate ICF and/or an inadequate procedure when determining the concentration of N^{+2} from the UV data.

2. Several distinct structures can be identified in IC 4593. Two inner nebulae, the outermost clearly elliptical, are surrounded by a nearly spherical and highly excited halo. These nebulae are obviously shaped by gas dynamical effects, whereas the halo bears the unmistakable appearance of being almost entirely dominated by photoionization. The inner nebulae may be related to episodic mass ejections.

3. If the ansae in IC 4593 were generated in the manner described by Socker (1992), their mass would imply they were produced in the post-AGB phase. Emission from low excitation lines is comparatively stronger in the ansae.

4. IC 4593 contains a large number of condensations, most of them located beyond the halo forming three separate "twisted strings". The most intriguing aspect of the system of condensations is that nearly all of them are located to the SW of the PNN. It remains to be discovered which is the origin of this asymmetric distribution.

5. The $H\beta$ flux is $\simeq 3.0 \times 10^{-11}$ erg cm^{-2} s^{-1} for the inner region and 3.1×10^{-11} erg cm^{-2} s^{-1} for the entire nebula. The ionized gas mass in the inner nebula is $\simeq 0.72(D_{kpc}/4.3)^2$ $M_\odot$, for a filling factor equal to unity.

6. Some physical properties in the inner nebulae are not uniform. Temperature, density and ion concentration in the innermost region display a regular pattern of variations in the azimuthal direction. The $H\beta$ flux has a peak towards the NW, otherwise is fairly uniform. In the intermediate region the $H\beta$ flux is also larger in this direction, but over a larger angle. [O III] 5007/$H\beta$ does not display the same variation pattern in the intermediate region.

7. Several properties of IC 4593 shed doubts on the hypothesis that the NW edge is being shaped by supersonic interaction with the ambient medium.

REFERENCES

Acker, A., Ochsenbein, F., Stenholm, B., Tylenda, R., Marcout, J., & Schohn, C. 1992, Strasbourg-ESO Catalogue of Galactic Planetary Nebulae

Aller, L.H. 1984, Physics of Thermal Gaseous Nebula, (Dordrecht: Reidel)

Aller, L.H., Keyes, C.D., Ross, J.E., & Czyzak, S.J. 1980, Ap&SS, 67, 349

Amnuel, P.R., Guseinov, O.H., Novruzova, H.I., & Rustamov, Yu.S. 1984, Ap&SS, 107, 19

Balick, B., Gonzalez, G., Frank, A., & Jacoby, G. 1992, ApJ, 392, 582

Barker, T. 1978, ApJ, 219, 914

Bohigas, J. 1988, A&A, 205, 257

Bohigas, J., López, J.A., & Aguilar, L. 1994, A&A, 291, 595

Cerruti-Sola, M., & Perinotto, M. 1989, ApJ, 345, 339

Clegg, R.E.S. 1987, MNRAS, 229, 31P

Cudworth, K.M. 1974, AJ, 79, 1384

Czyzak, S.J., Buerger, E.G., & Aller, L.H. 1975, ApJ, 198, 431

Dinerstein, H.L. 1980, ApJ, 237, 486

Freitas-Pacheco, J.A. de, Costa, R.D.D., Maciel, W.J., & Codina-Landaberry, S.J. 1989, An. Acad. Bras. Ci., 61, 389

French, H.B. 1983, ApJ, 273, 214

Hartigan, P., Raymond, J., & Hartmann, L. 1987, ApJ, 316, 323

Hutsemekers, D., & Surdej, J. 1989, A&A, 219, 237

Kaler, J.B. 1976, ApJS, 31, 517

Kazarian, M.A. 1968, in IAU Symp. 34, Planetary Nebulae, ed. D.E. Osterbrock & C.R. O'Dell (Dordrecht: Reidel), 381

Kingsburgh, R.L., & Barlow, M.J. 1994, MNRAS, 2, 2

Le Van, P.D., & Rudy, R.J. 1983, ApJ, 272, 137

López, J.A., Roth, M., & Tapia, M. 1993, A&A, 267, 194

Lutz, J.H. 1977, PASP, 89, 10

McCall, M.L. 1984, MNRAS, 208, 253

Méndez, R.H., Herrero, A., & Manchado, A. 1990, A&A, 229, 152

Miller, J.S., & Mathews, W.G. 1972, ApJ, 172, 591

Miranda, L.F., & Solf, J. 1992, A&A, 260, 397
Peimbert, M., & Torres-Peimbert, S. 1971, Bol. Obs.
    Tonantzintla y Tacubaya, 6, 21
Perinotto, M. 1974, A&A, 35, 293
Phillips, J.P., & Pottasch, S.R. 1984, A&A, 130, 91
Phillips, J.P., & Reay, N.K. 1983, A&A, 117, 33
Reynolds, R.J. 1991, in IAU Symp. 144, The Interstellar

Disk-Halo Connection in Galaxies, ed. H. Bloemen
    (Dordrecht: Kluwer), 67
Seaton, M.J. 1979, MNRAS, 187, 73P
Socker, N. 1992, ApJ, 389, 628
Torres-Peimbert, S., & Peña, M. 1991, Reporte Técnico
    No. 87, Instituto de Astronomía, UNAM
Zucker, D.B., & Soker, N. 1993, ApJ, 408, 579

Joaquín Bohigas: Observatorio Astronómico Nacional, Apartado Postal 877, 22830 Ensenada, B.C., México.
    (jbb@bufadora.astrosen.unam.mx)
Lorenzo Olguín: Instituto de Astronomía, UNAM, Apartado Postal 70-264, 04510 México D.F., México.
    (lorenzo@astroscu.unam.mx)